NeuroImage 72 (2013) 153–163

Contents lists available at SciVerse ScienceDirect

NeuroImage

journal homepage: www.elsevier.com/locate/ynimg

An unbiased longitudinal analysis framework for tracking white matter changes using diffusion tensor imaging with application to Alzheimer's disease

Shiva Keihaninejad [a,b], Hui Zhang [b,*], Natalie S. Ryan [a], Ian B. Malone [a], Marc Modat [a,b], M. Jorge Cardoso [a,b], David M. Cash [a,b], Nick C. Fox [a,1], Sebastien Ourselin [a,b,1]

[a] Dementia Research Centre, UCL Institute of Neurology, London, UK
[b] Centre for Medical Image Computing (CMIC), University College London, UK

ARTICLE INFO

Article history:
Accepted 13 January 2013
Available online 28 January 2013

Keywords:
Unbiased longitudinal image processing
Diffusion tensor imaging
Neurodegenerative diseases
Reliability and precision
Within-subject template

ABSTRACT

We introduce a novel image-processing framework for tracking longitudinal changes in white matter microstructure using diffusion tensor imaging (DTI). Charting the trajectory of such temporal changes offers new insight into disease progression but to do so accurately faces a number of challenges. Recent developments have highlighted the importance of processing each subject's data at multiple time points in an unbiased way. In this paper, we aim to highlight a different challenge critical to the processing of longitudinal DTI data, namely the approach to image alignment. Standard approaches in the literature align DTI data by registering the corresponding scalar-valued fractional anisotropy (FA) maps. We propose instead a DTI registration algorithm that leverages full tensor information to drive improved alignment. This proposed pipeline is evaluated against the standard FA-based approach using a DTI dataset from an ongoing study of Alzheimer's disease (AD). The dataset consists of subjects scanned at two time points and at each time point the DTI acquisition consists of two back-to-back repeats in the same scanning session. The repeated scans allow us to evaluate the specificity of each pipeline, using a test–retest design, and assess precision, using bootstrap-based method. The results show that the tensor-based pipeline achieves both higher specificity and precision than the standard FA-based approach. Tensor-based registration for longitudinal processing of DTI data in clinical studies may be of particular value in studies assessing disease progression.

Introduction

Diffusion tensor imaging (DTI) is a technique offering sensitivity to tissue microstructure of white matter (WM) (Basser and Pierpaoli, 1996; Pierpaoli et al., 1996). DTI is playing an increasingly important role in assessing white matter abnormalities in a variety of neurodegenerative disorders, including Alzheimer's disease (AD), vascular dementia (Hanyu et al., 1999; Sugihara et al., 2004), and frontotemporal dementia (Borroni et al., 2007; Matsuo et al., 2008). For example, in patients with AD, increased mean diffusivity (MD) and/or reduced fractional anisotropy (FA) compared to healthy controls have been reported for several white matter tracts, including the corpus callosum, cingulum bundle and fornix (Bozzali et al., 2002; Choo et al., 2010; Duan et al., 2006; Fellgiebel et al., 2008; Mielke et al., 2009; Oishi et al., 2011; Rose et al., 2000; Sexton et al., 2010).

Most DTI studies of neurodegenerative disorders have been cross-sectional in nature. Few investigate the changes in DTI measures as a function of disease progression. One notable exception is a longitudinal study of AD by Mielke et al. (2009), which showed that FA in the fornix, cingulum, splenium, and cerebellar peduncle remained stable in AD and healthy elderly subjects over a three-month follow-up. In contrast to many cross-sectional studies, which employ voxel-based analysis, Mielke et al. adopt region-of-interest (ROI) based analysis to provide the sensitivity necessary for detecting subtle temporal changes in white matter over a very short period of time. This suggests that ROI-based analysis, which trades reduced spatial specificity for improved sensitivity, may be an effective approach for measuring DTI changes due to disease progression.

The effectiveness of ROI-based analysis is dictated by the accuracy and consistency of ROI delineation across subjects. To date, most studies of this kind define WM ROIs manually. Manual delineation utilises expert knowledge in anatomy to ensure the accuracy of ROI definition. However, this is labour-intensive and time-consuming. Furthermore, it is also difficult to maintain a high-level of consistency for the entire dataset of a study, especially when placing the ROIs for small and thin tracts, such as the cingulum and the fornix, which are often plagued with partial volume effect with their surrounding anatomy. This becomes even more challenging for studies designed to track longitudinal changes. There is not only a need for between-subject consistency but also for within-subject between-scan consistency. This challenge motivates the present work.

* Corresponding author.
E-mail address: gary.zhang@ucl.ac.uk (H. Zhang).
[1] Joint senior author, the senior authors have contributed equally to the production of this manuscript.

1053-8119/$ – see front matter © 2013 Elsevier Inc. All rights reserved.
http://dx.doi.org/10.1016/j.neuroimage.2013.01.044

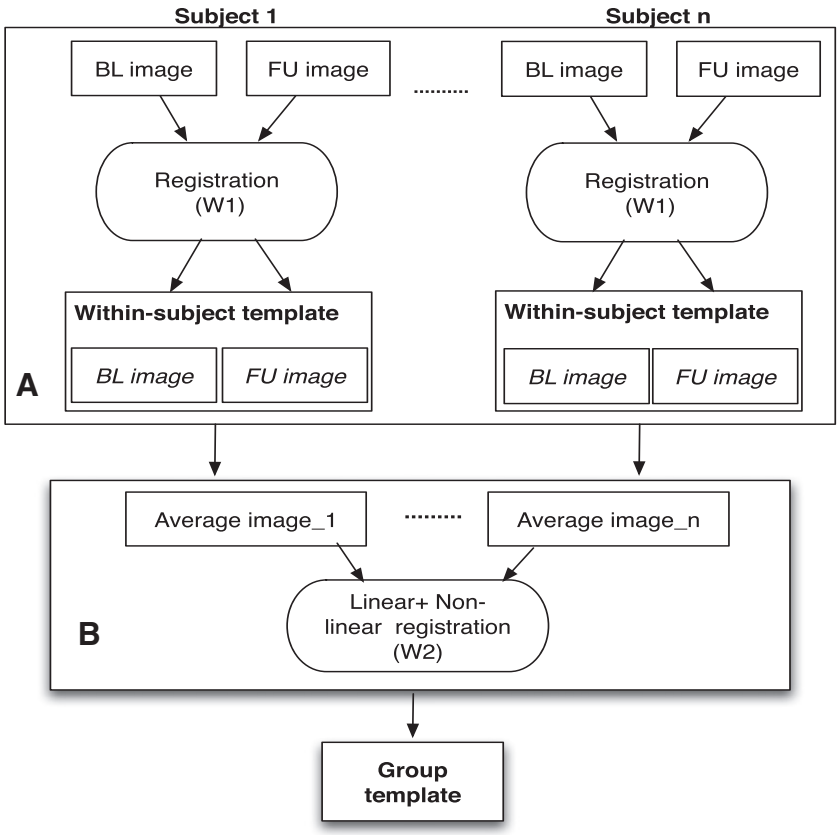

Fig. 1. Unbiased pipeline to study longitudinal changes in DTI parameters. Module A shows the step to create the unbiased within-subject template based on two time point images. Module B shows the step to create the group-wise atlas based on the within-subject templates. Details of registration methods and type of input images for Tensor_GW, FA_GW and FA_HS is shown in Table 1. BL = baseline, FU = follow-up.

In this paper, we propose an automated and unbiased DTI analysis pipeline for tracking longitudinal white matter changes. The pipeline aims to make ROI-based analysis both more accessible and more robust by combining best practices for unbiased longitudinal processing of structural imaging data (Reuter et al., 2012; Yushkevich et al., 2010) with recent advances in tensor-based image registration (Park et al., 2003; Zhang et al., 2006). We evaluate the performance of the proposed pipeline using data from an ongoing longitudinal study of AD and compare it against the more common approach of using FA-based image registration (Ardekani et al., 2007; Jones et al., 2002; Smith et al., 2006).

Materials and methods

Unbiased longitudinal DTI pipeline

Overview of the pipeline

The automated longitudinal processing pipeline is designed to enable a temporally unbiased evaluation of two time points where all time points of a subject are registered together to form a within-subject template. This is created in a mean space in order to avoid any interpolation asymmetry.

Interpolation asymmetries could arise when resampling follow-up images to the baseline scan (Yushkevich et al., 2010), as only the follow-up images are smoothed while the baseline image is unaffected. Module A of Fig. 1 illustrates the generation of an unbiased within-subject template for each subject in the study. The specific choice of registration method is discussed in the subsequent sections. The resulting template is unbiased towards any single time point. The original images, baseline and follow-up, are then transferred to this within-subject space and averaged. Module B of Fig. 1 demonstrates the creation of the group-wise (GW) atlas from the average images using iterative linear and non-linear registration methods. The mapping from the subject native space to its own within-subject template (warp field 1, W1, in Fig. 1) and the mapping from the within-subject template to the GW atlas (warp field 2, W2) were combined to create the deformation field that defines the mapping directly from the native space to the GW atlas.

Choices of registration methods

In this study, we propose that using a registration method that incorporates the entire tensor will provide more accurate and sensitive longitudinal measures than using FA based methods. For the tensor registration, we used a publicly available tool, DTI-TK,[2] for spatial normalisation of DTI data (Zhang et al., 2006). We compared the effectiveness of this method to a widely used FA-based method: all the linear and non-linear registrations were performed using FSL (Smith et al., 2004), FLIRT, FMRIB's linear image registration tool (Jenkinson and Smith, 2001) and FNIRT, FMRIB's Non-Linear Registration Tool (Andersson et al., 2007), with sum-of-squared differences as the cost function. Table 1 shows the detail of the unbiased longitudinal pipeline for each method.

Tensor-based pipeline. In the tensor-based registration pipeline, all linear and non-linear registrations were performed using DTI-TK on tensor images. By computing the image similarity on the basis of full tensor images rather than scalar features, the algorithm incorporates local fibre orientations as features that drive the alignment of individual WM tracts.

For each subject, a within-subject template was generated by computing the initial average template as a Log-Euclidean mean of the input DT images from the two time points. The Log-Euclidean tensor

[2] http://dti-tk.sourceforge.net.

Table 1
Comparison of key aspects between the three approaches of the longitudinal pipeline described in Fig. 1: Tensor_GW, FA_GW and FA_HS.

	Tensor_GW	FA_GW	FA_HS
Type of input image	Tensor	FA	FA
Within-subject reg (W1)	Linear, non-linear	Linear, non-linear	Linear
Group template reg (W2)	GW linear, non-linear	GW linear, non-linear	Linear, non-linear to FMRIB58_FA

averaging preserves WM orientation with minimal blurring (Arsigny et al., 2006). The template was iteratively refined through the following steps: the DT images are registered to the template and a refined template is computed as an average of the registered DT images for the next iteration. The process is repeated until the change between templates from consecutive iterations becomes sufficiently small, first with affine and then with non-linear registrations (Zhang et al., 2007a, 2007c). The Euclidean distance of tensors (overall distance between measures) is the metric used during the affine stage and the Euclidean distance of deviatoric tensors (difference between the anisotropic components of the tensors) is the metric used during the non-linear stage. The former metric was chosen for the affine registration as it is more stable over a larger capture range. Once a suitable affine alignment has been established, the latter metric provides a more accurate non-linear alignment between different white matter tracts (Zhang et al., 2006). Then a GW atlas is created from all of the average images in the within-subject space using the described iterative method. Maps of FA, MD, axial (DA) and radial (RD) diffusivity were created from the GW atlas and each registered tensor image in the GW atlas space. This pipeline will be referred to as the Tensor_GW method in this study.

FA-based pipeline. Two pipelines were designed to investigate the FA-based approach:

- Group-wise FA (FA_GW): This pipeline is the same as the Tensor_GW method but the FA based image registration is used instead to create the within-subject template and GW atlas (Keihaninejad et al., 2012).
- Half-way space FA (FA_HS): In order to do a comparison with established techniques, we applied the method proposed by Zatorre et al. (2012). For each subject, the FA maps of two time points were registered to a space mid-way between the spaces of two images using an affine transformation, and averaged. The generated templates were then non-linearly aligned to FMRIB58_FA in standard space and averaged to generate a study-specific template. The FA maps in the native space were then transformed to standard space by combining the linear transform to the half-way space with the transform from that half-way space to standard space.

Atlas-based ROI segmentation

To include the major WM tracts, the FA map of the GW atlas is segmented using the LoAd (Locally Adaptive) tool, which is part of the NiftySeg[3] package (Cardoso et al., 2011). A binary mask was created using a threshold of 50% on the WM probability map in order to focus on areas that were likely to be predominantly WM.

The ICBM-DTI-81 white matter labels and tract atlas, developed by Johns Hopkins University (JHU) was used to locate the WM tracts of interest (Mori et al., 2005). To be consistent and avoid bias toward the registration technique used in FLIRT and FNIRT, the FA map of the JHU atlas was linearly and non-linearly registered to the final template FA map using NiftyReg[4] (Modat et al., 2010). This transformation was used to warp the labels from the WM atlas to the template FA image through nearest neighbour interpolation. In this study, we focused on six white matter ROIs: the genu, body, and splenium of the corpus callosum, as well as the fornix and cingulum bundles (left and right). Each ROI was combined with the binary WM mask to remove voxels that did not contain sufficient white matter. An example of the ROIs overlaid onto an individual subject using the three methods can be found in Fig. 2. These are the most common white matter ROIs where the literature indicates a change in structures between those with AD and controls (Douaud et al., 2011; Duan et al., 2006; Fellgiebel et al., 2008; Rose et al., 2000). The fornix as the major outflow tract of the hippocampus is very relevant to AD as is the cingulum, since both the hippocampus and posterior cingulate are early sites of AD involvement (Scahill et al., 2002).

Experimental evaluation

We evaluated and compared the above methods, Tensor_GW, FA_GW, and FA_HS using what we refer to below as “specificity” and “sensitivity” experiments. We also applied the tensor-based registration method on a cross-sectional dataset in order to validate that the proposed method was identifying similar differences between AD and controls as other widely used techniques.

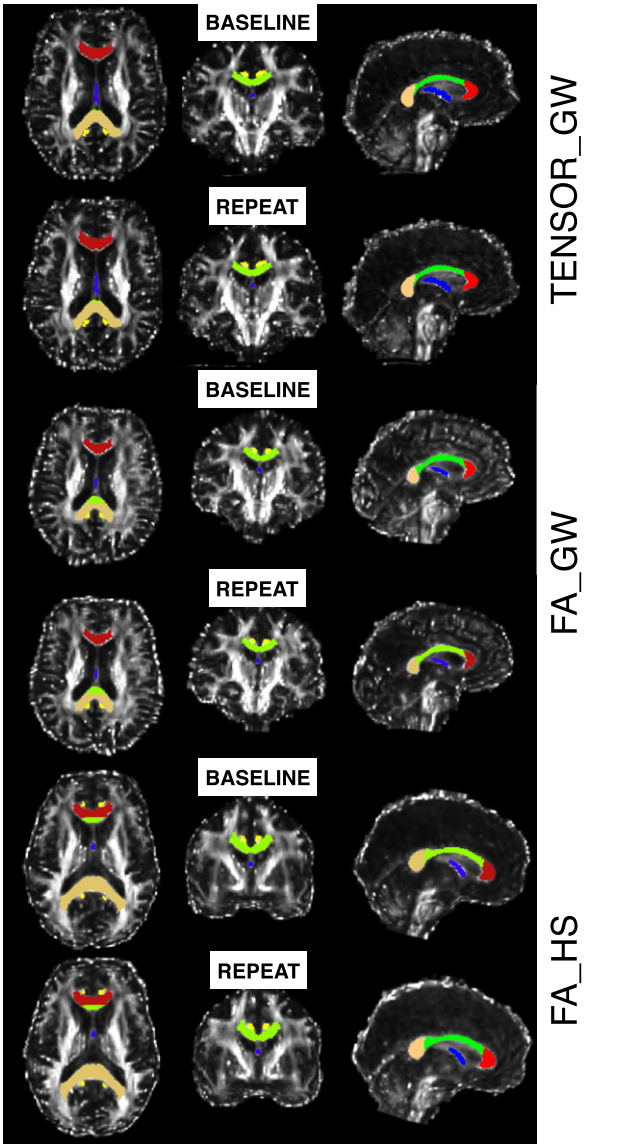

Fig. 2. Resulting ROI overlays using the different registration methods for an example AD subject. The ROIs illustrated here are: genu (red), body (green) and splenium (tan) of the corpus callosum, fornix (blue) and left and right cingulum (yellow). The ROIs are defined in the final group wise atlas space, so they are consistent for each time point.

[3] http://sourceforge.net/projects/niftyseg.
[4] http://sourceforge.net/projects/niftyreg.

Specificity experiment

Test–retest data was analysed in this experiment. This dataset consists of 11 AD patients (4 women; mean ± sd age: 60.8 ± 6.3 years; Baseline MMSE score: 23.3 ± 4.5) and 12 controls (10 women; age: 56.5 ± 8.6 years; MMSE score: 29.7 ± 0.7) each scanned twice back-to-back within the same session and will be referred to as test–retest dataset, *TT-23*. There was no significant difference between AD subjects and controls in mean age, but there was a higher proportion of women in the control group (Fisher's exact test $p = 0.03$). All subjects gave written informed consent and the study had local ethics committee approval. The patients had all been assessed in the Cognitive Disorders Clinic at the National Hospital for Neurology and Neurosurgery in London, where they had been given a clinical diagnosis of AD. These two DTI scans are used to evaluate the reliability of the proposed methods.

Sensitivity experiment

To study group discrimination power and robustness of different processing streams we analyse the same dataset as *TT-23* when subjects had a follow-up scan in 13.2 ± 2.1 months and will be referred to as longitudinal study dataset, *LS-23*. All subjects underwent clinical assessment, neuropsychological testing, and MRI scanning both at baseline and follow-up.

Since each subject in *LS-23* had two scans at each visit, we divided the scans into four combinations in order to study the robustness of different approaches:

1. *B1-F1*: baseline first scan with follow-up first scan
2. *B1-F2*: baseline first scan with follow-up second scan
3. *B2-F1*: baseline second scan with follow-up first scan
4. *B2-F2*: baseline second scan with follow-up second scan

The null hypothesis would be that there would be no difference between the measurements of change for any combination of any two of these longitudinal scan-pairs.

Cross-sectional experiment

Twenty-two AD patients (11 women; mean ± sd age: 61.9 ± 5.0 years; Baseline MMSE score: 20.7 ± 5.5) and eighteen controls (12 women; age: 57.8 ± 10.4 years; Baseline MMSE: 29.7 ± 0.6) were included in the cross-sectional study and will be referred as cross-sectional study dataset, *CS-40*. AD subjects and controls were not significantly different in mean age ($p = 0.14$, two-tailed t-test with unequal variance) and gender distribution ($\chi^2(1)$ test statistic = 1.7988, $p = 0.18$).

The baseline scans from subjects of *LS-23* dataset were part of the *CS-40*. 12 subjects had not had a follow-up scan and the follow-up scans of five subjects, four control and one AD participant, had significant scanner related artefact. Details of subject demographics for the longitudinal dataset (LS-23/TT-23) and the cross-sectional data set (CS-40) can be found in Table 2.

The pipeline for the cross-sectional study using tensor-based registration is similar to the Tensor_GW pipeline except that no within-subject template could be created, so the first step was creating the GW atlas from all subjects. All of the DTI parameter maps were created from the GW atlas and the images transformed into group-wise space in a similar manner, as were the ROIs used for analysis.

Table 2
Subject demographics and cognitive data. * indicates that one AD subject's MMSE was not available at the time of the second scan.

	Longitudinal Control	Experiment AD	Cross-sectional Control	Experiment AD
N	12	11	18	22
Age (years)	56.5 (8.6)	60.8 (6.3)	57.8 (10.4)	61.9 (5.0)
Gender (M/F)	2/10	7/4	6/12	11/11
MMSE at scan 1	29.7 (0.7)	23.3 (4.5)	29.7 (0.6)	20.7 (5.5)
MMSE at scan 2*	29.3 (0.9)	20.0 (5.1)	N/A	N/A
Interval between scans (years)	1.1 (0.2)	1.1 (0.2)	N/A	N/A

Image acquisition

All the participants received a whole-brain T1-weighted and diffusion-weighted scan acquired on the same 3 Tesla scanner (Siemens Tim Trio) using the same 32-channel head coil.

The 3D T1-weighted images were acquired using an MP-RAGE sequence with the following parameters: sagittal slices, matrix 256×256, 208 slices, 1.1 mm in-plane resolution, slice thickness = 1.1 mm, TE/TR = 2.9/2200 ms, TI = 900 ms, flip angle = 10°.

Diffusion-weighted images were obtained on the AD and control cohorts (first and second time points) using echo-planar imaging (SE-EPI, TE/TR = 91/6900 ms, 96×96 acquisition matrix and 55 slices, 2.5 mm isotropic voxels) with 64 isotropically distributed orientations for the diffusion-sensitising gradients at a b-value of 1000 s/mm^2 and one $b = 0$ (b_0) image. An extra set of 7 b_0 images were acquired to improve signal to noise. For each visit of subjects in *CS-40* and *LS-23* dataset, a second set of weighted images with the same 64 sensitising gradients and one $b = 0$ was acquired immediately after the first sequence.

Images were affinely registered to the first unweighted volume with FLIRT to correct for motion and eddy currents and the weighting vectors adjusted for rotation. Diffusion tensors were fitted with the Camino package (Cook et al., 2006) using all acquired volumes.

Statistical analyses

As mentioned above, the unbiased longitudinal DTI pipeline avoids interpolation asymmetry induced bias by treating all time points equivalently. Another source of processing bias can be due to the registration of the scalar features.

As a dimensionless measure of change we compute the percent change (PC) of the FA of a ROI with respect to the average FA defined as:

$$PC = 100\frac{(FA_2 - FA_1)}{0.5(FA_1 + FA_2)} \quad (1)$$

where FA_i is the FA of scan i, where i could either be referring to first or second acquisition in the case of *TT-23* or the first or second time point in the case of *LS-23*.

To quantify test–retest reliability we used the intraclass correlation coefficient (ICC) measure of FA (Bartlett and Frost, 2008). The ICC value quantifies the consistency and reliability of the repeated scans.

The annualised rate of change in DTI metrics was computed as the DTI parameter value of the follow-up scan minus that of baseline scan divided by the duration between the two scans (in years). To compare the annualised rate of change between AD cases and controls, the linear regression model was used adjusting for baseline age and gender.

As mentioned in Section 2, two back-to-back scans were acquired at each time point. The longitudinal percentage FA change can be computed between the 4 possible combinations of the back-to-back scans: 1: B1-F1; 2: B1-F2; 3: B2-F1; and 4: B2-F2. In order to identify potential bias or variability in the change measurement between any of these scan combinations, we took the difference between the change measurements coming from these 4 scan combinations to generate 6 pairs of difference measurements (i.e. 1−2, 1−3, 1−4, 2−3, 2−4, and 3−4). We performed paired t-tests between the 6 difference measurements to determine if the percentage FA change was significantly different between these 6 difference measurements ($p < 0.05$).

In the cross-sectional analysis of the baseline scans, linear regression models were used to assess differences in DTI metrics of white matter tracts between patients and controls adjusting for age and gender. All

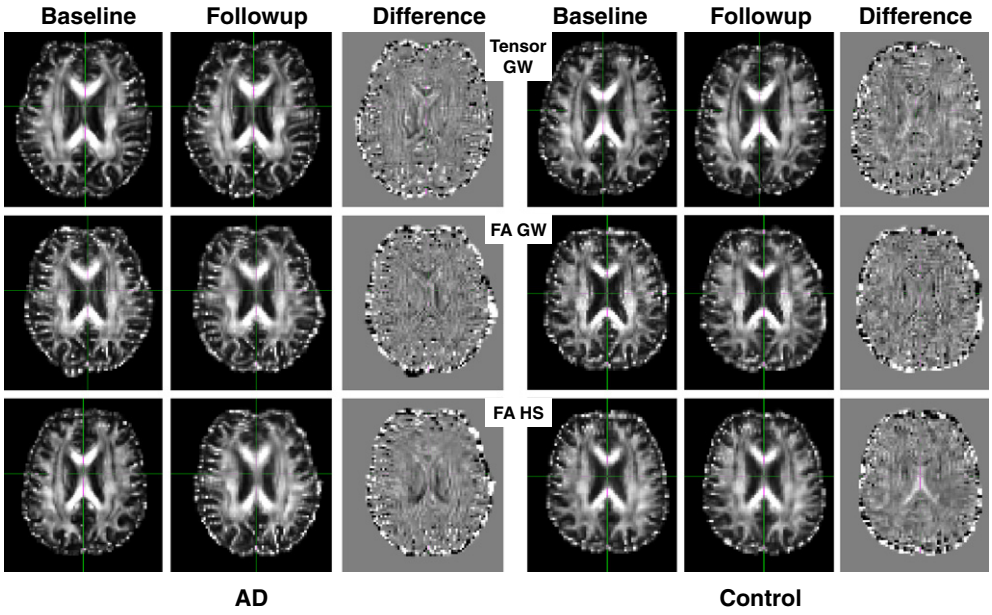

Fig. 3. Comparison of intra-subject registration approaches for two example subjects: one AD patient (left) and one control (right). All FA images have been normalised to an intensity window of 0 to 0.7, while the difference images have an intensity display window of −0.1 to 0.1. There are very clear misregistrations present on the FA_HS method in the corpus callosum.

analyses were done using Stata 12.0 (Stata, College Station, TX) and considered p values of <0.05 significant for all analyses.

Results

Registration assessment

Figs. 3 and 4 illustrate the effects of the three different methods on the within-subject template step (W1) and the between-subject group-wise atlas construction step (W2). It is clear that there are within-subject misregistrations in the corpus callosum region that are most apparent when using the FA_HS method. In the FA_HS method, only a linear registration method is used, which is incapable of recovering non-linear changes that occur between visits. These changes could not only be due to atrophy, but also due to changes in positioning and head orientation between visits. For the inter subject registration, the group wise atlas resulting from the TENSOR_GW technique provides more clearly delineated white matter anatomy than the two methods based on FA. When using all of the tensor information, the registration technique can align between subjects the boundaries of two adjacent tracts that have similar FA but different orientation. Once the information is compressed into a non-directional metric like FA, there is no longer the ability to resolve this information.

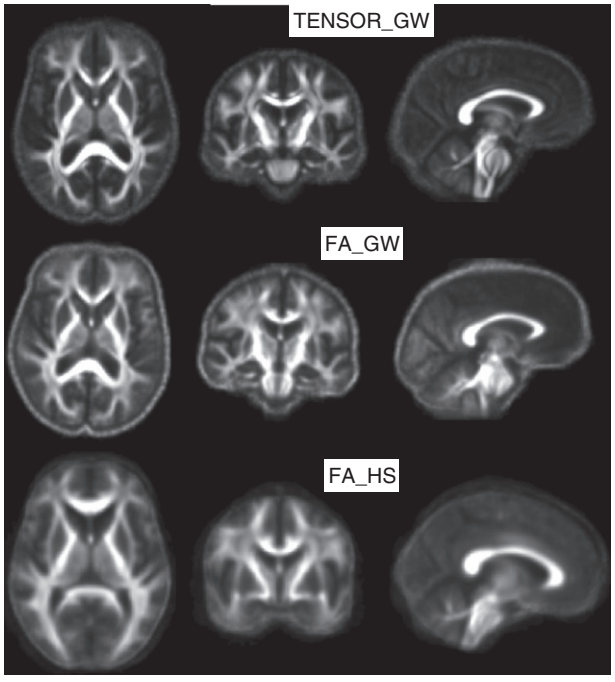

Fig. 4. Comparison of group-wise atlas methods by the three approaches. The FA atlas using the TENSOR_GW technique provides a sharper atlas than the other two methods indicating that the tensor-based method provides better alignment between subjects.

Specificity experiment

Fig. 5 shows the percentage change in FA for different structures when processing the test–retest data with FA-based and tensor-based approaches. As the scans are performed back to back, it would be expected that the average change in each structure would be close to zero. In the *TT-23* set, nonzero average changes that were significant were found using both the FA_GW and FA_HS methods for the body and splenium of the corpus callosum and the cingulum bundle.

It can be observed in Fig. 5 that the proposed processing stream based on tensor registration shows a much lower level of FA difference between the test–retest scan; the differences were not significantly different from zero for any of the ROIs. This suggests the tensor registration is more robust to bias between the first and second acquisitions than either the FA_HS or FA_GW pipelines.

The test–retest reliability, in terms of ICCs between repeated scans is shown in Table 3. The ICC value is greater than 0.99 for all the white matter ROIs when using Tensor_GW.

Sensitivity experiment

An assessment of differential change between baseline and follow-up when using Tensor_GW method showed the annualised change in FA was significantly different between AD and controls for the genu, body and left cingulum bundle (Table 4). For MD, the change

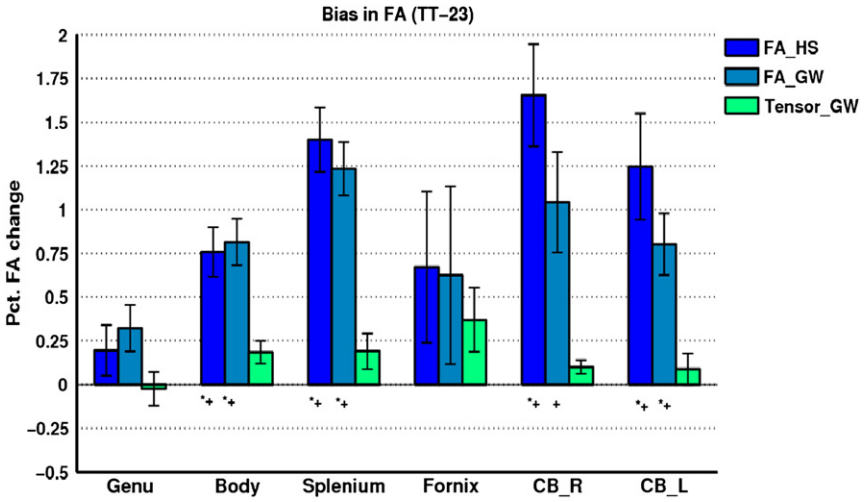

Fig. 5. Percentage change in FA is shown based on different approaches. FA-based approaches clearly show a bias in percent change. Using the tensor-based method does not show a significant difference between repeated scans in the test–retest dataset, *TT-23*. The mean percentage change of FA is shown with standard error (standard deviation divided by square root of the sample size). Significant differences from zero ($p<0.05$) are denoted by + for controls and *for AD subjects.

was significantly different between AD and controls for the genu, body and fornix. The annualised change of axial diffusivity was significantly different between the two groups for the genu and body of corpus callosum, while significant differences in annualised change of radial diffusivity was observed in the genu, body and fornix.

FA_HS and FA_GW methods showed higher variation in the annualised change of FA in both groups compared to Tensor_GW. FA_HS showed no significant difference on annualised change of FA between AD and controls but in MD of the genu, body, splenium and fornix. FA_GW showed significant difference for the annualised change of FA in the splenium and left cingulum and in MD for the body of corpus callosum.

Fig. 6 shows plots of percent change averages (and standard errors). Higher ability to distinguish the AD from the normal control group based on the percent FA change can be seen mainly in the genu, body and cingulum bundle when using Tensor_GW.

Figs. 7 and 8 show the variability of longitudinal change of FA as percent change in *LS-23* when different scan combinations of baseline and follow-up are studied using different longitudinal approaches. The results of the performed paired t-test between 4 scan combinations, 6 possible pairs of comparison, are shown in inset 4×4 matrix for each structure and each method. Each 4×4 matrix indicates the combinations that showed statistically significant difference with other combinations. The lower triangle of the 4×4 matrix indicates which of these 6 combinations was significant for AD, the upper triangle for controls. The significant result ($p<0.05$) is coloured for each group, AD in green, controls in yellow and blank shows there is no significant difference in the paired t-test. Diagonals are colour coded red as combinations are not tested against themselves and also to serve as a boundary between AD and controls.

Figs. 7 and 8 show that the Tensor_GW approach results in the same FA longitudinal change in the controls and AD group regardless of which scan combinations are used, which confirms the robustness of this pipeline. For the Tensor_GW, the only significant difference was found between B1-F2 and F1-B2 on the splenium of corpus callosum. FA_HS shows the most biased results when using different scan combinations for both groups and all the ROIs except the fornix. FA_GW shows the same pattern of bias but less than FA_HS.

Table 3
The reliability of the repeated scans analysed with three methods is measured using the ICC.

White matter ROIs	Tensor_GW	FA_GW	FA_HS
Genu	0.996	0.991	0.992
Body	0.997	0.983	0.986
Splenium	0.990	0.934	0.931
Fornix	0.997	0.987	0.995
Cingulum_R	0.999	0.958	0.953
Cingulum_L	0.997	0.984	0.959

Cross-sectional experiment

Using a linear regression model and calculating the cross-sectional associations, there were three ROIs in which FA differed at baseline between the AD and control groups, controlling for age and gender. Compared to controls, AD subjects had lower mean FA in the genu of corpus callosum, fornix and bilateral cingulum bundle (Table 5). AD patients had increased MD in all the white matter ROIs examined in this study. AD subjects had also higher axial and radial diffusivity compared to controls in all the white matter ROIs except the left cingulum and splenium, respectively.

Discussion

The creation of a robust within-subject template yields an initial unbiased estimate of the location of anatomical structures for a longitudinal scheme. Our approach of treating all time points the same removes interpolation asymmetry induced processing bias. The tensor based registration method using DTI-TK provided significant improvements to the unbiased longitudinal pipeline that reduced bias in the specificity experiments but also increased the ability to detect real change in the sensitivity experiments. The motivation for using diffusion-tensor data to drive the registration is that the orientational information potentially provides powerful features for matching. Using full-tensor information as a similarity metric for non-linear warping has been shown to be effective in spatially normalising tract morphology and tensor orientation (Park et al., 2003; Wang et al., 2011; Zhang et al., 2006).

In the specificity experiment, the Tensor-GW method was the only one of three to show no significant FA change between two repeated scans. It also improves the reliability measured by ICC. However, there is potential bias occurring in the test–retest experiment due to several kinds of artefacts, including head motion artefact, bed vibration artefact, etc. Although no correction for multiple comparisons (due to the multiple ROIs) has been performed, the main goal of these values is only to demonstrate that a clear trend exists concerning

Table 4
Annualised change (mean ± SD) for AD patients and normal controls (NC): each difference score (follow-up − baseline) was divided by the scan interval to create a rate of change (slope). Values were multiplied by 1000 to reduce the number of decimal figures.

White matter ROIs	AD (n = 11)			NC (n = 12)		
	FA_HS	FA_GW	Tensor_GW	FA_HS	FA_GW	Tensor_GW
FA						
Genu	−0.96 ± 13.91	−10.89 ± 14.67	−9.79 ± 7.77‡‡	3.94 ± 8.72	−0.66 ± 7.45	−0.20 ± 5.83
Body	−3.18 ± 11.08	−5.89 ± 11.96	−8.30 ± 9.74‡‡	6.00 ± 8.27	1.78 ± 7.44	5.04 ± 6.34
Splenium	−1.87 ± 11.63	−7.69 ± 9.95 ††	−5.38 ± 6.58	4.21 ± 7.84	2.34 ± 5.91	0.76 ± 3.97
Fornix	−22.73 ± 22.05	−35.79 ± 33.72	−22.65 ± 18.77	−3.33 ± 22.30	−13.95 ± 32.45	−8.73 ± 13.23
Cingulum_R	11.38 ± 20.83	−14.37 ± 12.52	−8.55 ± 12.17	4.30 ± 12.49	−3.22 ± 14.42	−2.51 ± 7.88
Cingulum_L	9.74 ± 19.55	−14.55 ± 11.94†	−6.95 ± 12.16‡	7.12 ± 11.50	−5.93 ± 9.54	0.30 ± 6.75
MD						
Genu	29.90 ± 36.16*	14.89 ± 22.55	21.73 ± 21.04‡‡	4.05 ± 13.06	7.04 ± 14.54	−0.04 ± 9.76
Body	49.49 ± 45.25*	9.07 ± 14.96†	11.72 ± 20.05‡‡	−1.14 ± 24.17	−9.73 ± 16.46	−11.29 ± 11.98
Splenium	59.49 ± 51.02**	7.25 ± 13.02	13.94 ± 20.01	−3.02 ± 20.84	−5.68 ± 14.58	−1.45 ± 12.68
Fornix	86.62 ± 55.55**	90.77 ± 98.42	98.11 ± 70.15‡‡	1.18 ± 63.63	45.78 ± 75.25	26.07 ± 36.43
Cingulum_R	1.95 ± 24.17	21.08 ± 32.99	17.06 ± 21.76	2.90 ± 19.60	13.84 ± 19.98	7.51 ± 17.89
Cingulum_L	−3.47 ± 23.34	24.99 ± 30.74	20.28 ± 29.16	−5.53 ± 20.18	9.68 ± 20.50	12.19 ± 17.40

R: Right; L: Left; AD vs. NC using FA_HS (*,**), FA_GW (†,††), Tensor_GW (‡,‡‡); *,†,‡:$p<0.05$; **,††,‡‡:$p<0.01$.

the specificity of each of the techniques that we evaluate. Our results with the tensor-based technique are supported by the findings of Pfefferbaum et al. (2003), where they evaluated within-scanner and between-scanner reliability of FA in 10 subjects who had three scans on two different scanners. Using a voxel-by-voxel analysis of all supratentorial brain (gray matter + white matter + cerebrospinal fluid) and a single-region analysis of the corpus callosum, they found that FA correlation was equivalently and significantly higher within than across scanners.

Despite a growing interest in the use of DTI to characterise neurodegenerative diseases, such as AD, there have been relatively few studies looking at longitudinal changes in white matter integrity in the presence of AD or other degenerative diseases (Mielke et al., 2009; Teipel et al., 2010). Mielke et al. studied the FA and MD changes over 2.5 years in the fornix and cingulum bundle and their correlation to hippocampal volume and memory decline (Mielke et al., 2012) using the same manual delineation protocol used in Mielke et al. (2009). With the previously used ROI-based methods as utilised in Mielke et al. (2009), it is difficult to objectively and reproducibly place ROIs on small or thin tracts on the images of individual patients, when the slice orientation and anatomical details (such as atrophy) may show variation between individuals at two or more time points and when the boundaries of the white matter tracts are not easily identified. There is also variability arising between different time points when creating a half-way or group-wise space based on FA images because of some misalignment.

To the best of our knowledge, group-wise based methods (both FA_GW and Tensor_GW) proposed in this study have not previously been used for longitudinal DTI analysis. They have a number of

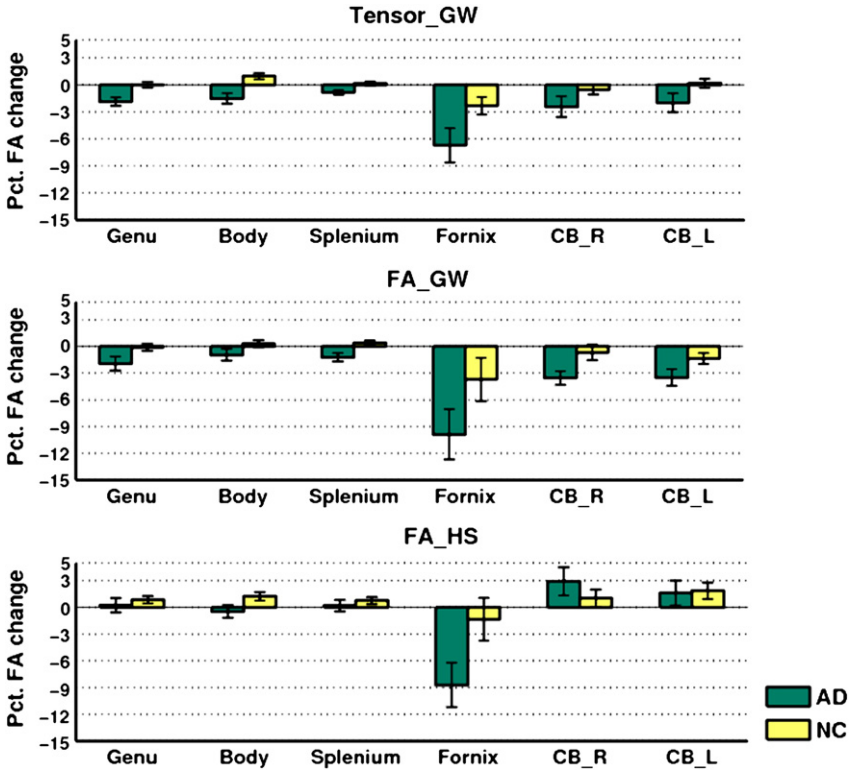

Fig. 6. Percent FA change of the longitudinal *LS-23* dataset for Tensor_GW (top); FA_GW (middle) and FA_HS (bottom) processing.

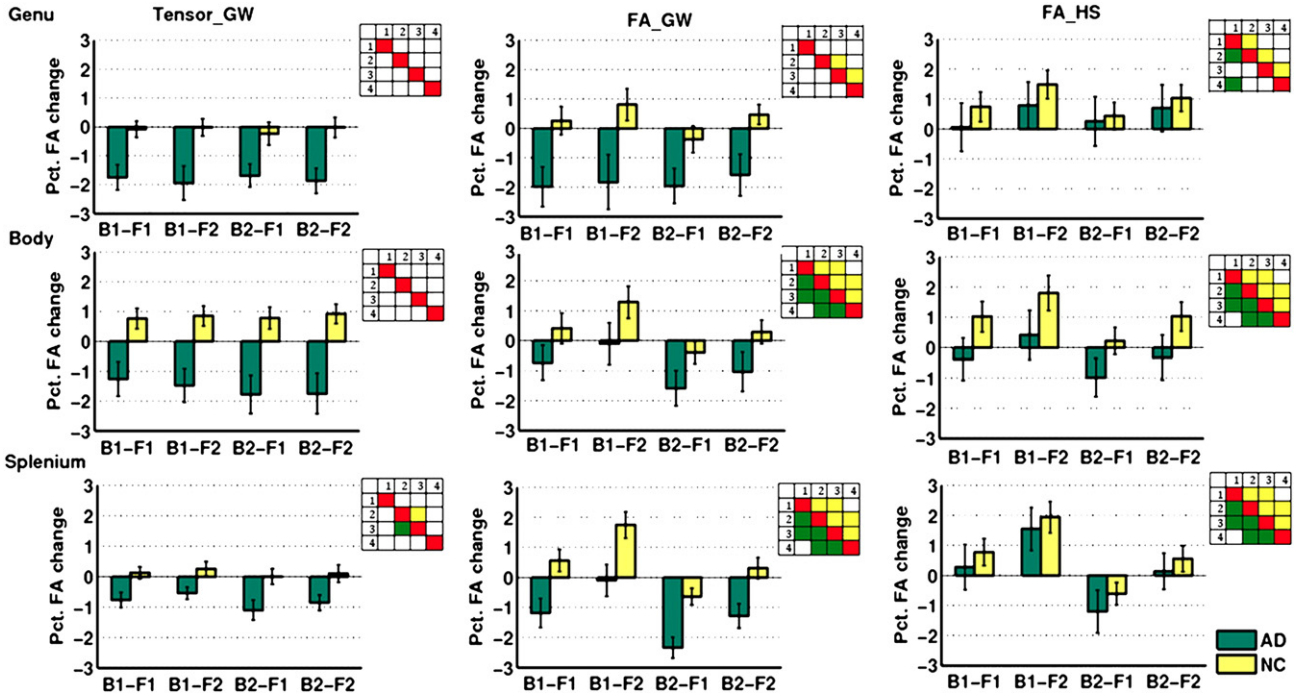

Fig. 7. Percent FA change of the *LS-23* dataset on different baseline follow-up scan combinations using Tensor_GW, FA_GW and FA_HS pipeline in the genu, body and splenium of the corpus callosum. Paired t-test was performed between each of the combinations to determine if the difference between the percent FA changes was significantly different ($p<0.05$), resulting in 6 total tests each for AD and controls. The inset in each graph is a 4×4 matrix which indicates the combinations that achieved statistically significant difference (1 = B1F1, 2 = B1F2, 3 = B2F1, 4 = B2F2). The lower triangle of the 4×4 matrix shows the results for AD, the upper triangle for controls. Diagonal are colour coded in red as combinations are not tested against themselves. B: baseline, F: follow-up, 1: first scan, 2: second scan, L: Left, R:Right.

advantages over the FA_HS method. First, there is no limitation with regards to processing only two time points. Second, non-linear within-subject registration can deal with the atrophy that may occur between time points in a longitudinal study. Third, creating an inter-subject group-wise atlas eliminates the potential for bias when spatially normalising elderly controls and AD patients, compared to a standard template of adult subjects such as FMRIB58_FA. We show this third benefit for voxel-based analyses in a recent study (Keihaninejad et al., 2012) that uses a method nearly identical to the FA_GW method. In this study, we further illustrate, through

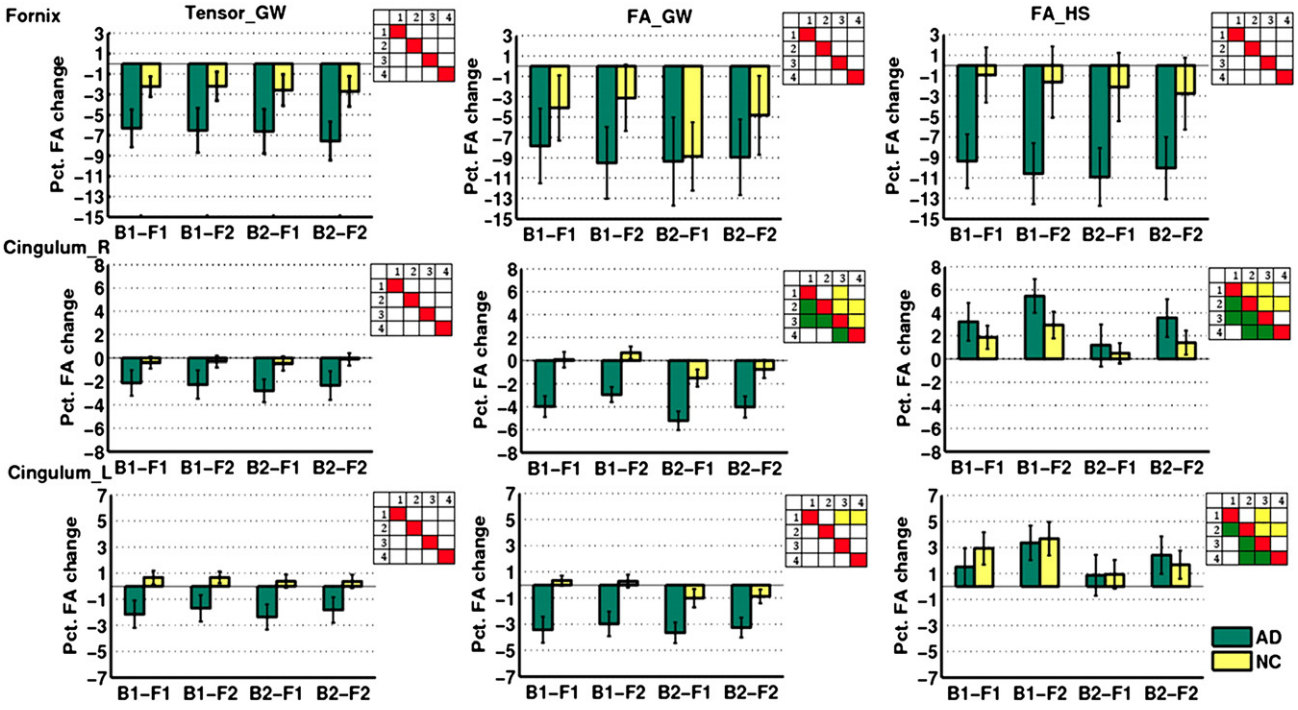

Fig. 8. As in Fig. 7 but the fornix, right and left cingulum.

Table 5
Descriptive statistics of FA, MD, DA and RD (mean ± SD); significance for comparison between subject groups; the 95% confidence intervals (CI) for the adjusted differences between group means (the mean for the patient group minus the mean for the healthy group).

White matter ROIs	NC (n = 18)	AD (n = 22)	Adjusted difference (95%CI)	P-value
FA (raw values)				
Genu (CC)	0.601 ± 0.035	0.562 ± 0.036	−0.032 (−0.056,−0.009)	0.006
Body (CC)	0.590 ± 0.035	0.571 ± 0.034	−0.015 (−0.038, 0.007)	0.186
Splenium (CC)	0.659 ± 0.032	0.643 ± 0.026	−0.011 (−0.029, 0.006)	0.206
Fornix	0.411 ± 0.041	0.353 ± 0.042	−0.044 (−0.071,−0.018)	0.001
Cingulum bundle R	0.456 ± 0.028	0.418 ± 0.031	−0.032 (−0.051,−0.013)	0.001
Cingulum bundle L	0.445 ± 0.033	0.413 ± 0.031	−0.027 (−0.047,−0.007)	0.009
MD (10^{-3} mm^2/s)				
Genu (CC)	0.866 ± 0.045	0.970 ± 0.074	0.086 (0.040, 0.133)	0.001
Body (CC)	0.879 ± 0.047	0.940 ± 0.064	0.051 (0.008, 0.093)	0.021
Splenium (CC)	0.904 ± 0.068	0.975 ± 0.061	0.053 (0.007, 0.099)	0.023
Fornix	1.758 ± 0.204	2.037 ± 0.160	0.211 (0.100, 0.322)	0.001
Cingulum bundle R	0.817 ± 0.034	0.902 ± 0.061	0.074 (0.036, 0.112)	<0.001
Cingulum bundle L	0.802 ± 0.057	0.880 ± 0.084	0.059 (0.004, 0.113)	0.034
DA (10^{-3} mm^2/s)				
Genu (CC)	1.563 ± 0.039	1.664 ± 0.070	0.079 (0.038, 0.120)	0.001
Body (CC)	1.572 ± 0.047	1.631 ± 0.059	0.043 (0.004, 0.083)	0.030
Splenium (CC)	1.702 ± 0.078	1.796 ± 0.068	0.073 (0.021, 0.125)	0.007
Fornix	2.560 ± 0.189	2.814 ± 0.160	0.172 (0.064, 0.280)	0.003
Cingulum bundle R	1.259 ± 0.037	1.312 ± 0.048	0.050 (0.020, 0.081)	0.002
Cingulum bundle L	1.214 ± 0.053	1.263 ± 0.072	0.033 (−0.013, 0.079)	0.158
RD (10^{-3} mm^2/s)				
Genu (CC)	0.517 ± 0.052	0.625 ± 0.077	0.090 (0.040, 0.140)	0.002
Body (CC)	0.532 ± 0.054	0.595 ± 0.069	0.054 (0.006, 0.102)	0.026
Splenium (CC)	0.505 ± 0.066	0.566 ± 0.058	0.043 (−0.000, 0.088)	0.054
Fornix	1.356 ± 0.212	1.681 ± 0.174	0.231 (0.113, 0.348)	<0.001
Cingulum bundle R	0.596 ± 0.038	0.697 ± 0.072	0.086 (0.042, 0.131)	<0.001
Cingulum bundle L	0.595 ± 0.064	0.688 ± 0.094	0.072 (0.011, 0.133)	0.022

CC: corpus callosum; R: right; L: left; NC: normal controls.

the sensitivity and specificity experiments, that the unbiased longitudinal pipeline using tensor information significantly improves precision of studying longitudinal change based on DTI. In this study, we focussed on using ROI based measures such as the ones used by Mielke et al. (2012) to provide similar quantitative measures to those that are currently in the literature and have potential utility in the clinic. In future work we hope to apply the Tensor_GW method to voxel-based techniques, such as TBSS, to see if it can improve the results that were obtained using FA_GW.

Further, we studied different scan combinations on longitudinal change of FA when either first acquisition or second one is employed as the longitudinal dataset. Both FA-based approaches showed significant differences in the change of key DTI metrics, such as FA, based on different scan combinations. One scan in the visit should not provide any systematically different results from another. The tensor-based approach showed the fewest significant differences between different baseline and follow-up scan combinations for the WM ROIs. Only the splenium of the corpus callosum was significantly different between B1-F2 and B2-F1. This difference was in the same direction as the significant differences for FA_HS and FA_GW in the test–retest experiments, suggesting a small bias between the first and second diffusion acquisitions which the tensor registration is more reliably able to reject.

The cross-sectional experiment demonstrated significant differences in fiber tract integrity (as measured by FA) in AD vs. controls in the genu of the corpus callosum, fornix and the cingulum bundle bilaterally. Whilst a reduced FA and/or an increased MD in the corpus callosum is one of the most consistent findings in AD (Douaud et al., 2011; Liu et al., 2011), there has been conflicting evidence about whether the genu (Head et al., 2004; Xie et al., 2006) or the splenium (Rose et al., 2000; Takahashi et al., 2002) shows the greatest neuropathological change. These conflicting results may be due to differences in the selection of patient populations. In our study, we found a decrease in FA in the genu accompanied by an increase of MD in the genu, body and splenium. The reduced FA in the bilateral cingulum is consistent with other studies (Catheline et al., 2010; Ding et al., 2008; Kiuchi et al., 2009; Mielke et al., 2009; Nakata et al., 2008; Takahashi et al., 2002; Zhang et al., 2007b). The increases of MD in the corpus callosum, fornix and cingulum were also supported by other research (Agosta et al., 2011; Douaud et al., 2011; Duan et al., 2006). In the event of concomitant (but not quite significant) increases in both axial and radial diffusivity, MD provides a pooled measure that may be statistically more sensitive than either of the individual component measures.

Our dataset in this study was limited to two time points. The proposed unbiased longitudinal processing based on the tensor information can however be extended to evaluate scans that have been collected at more than two time points. The regions of interest which showed a significant change in diffusivity metrics over one year (namely the fornix, left cingulum and genu and body of corpus callosum) in the AD patients were all already significantly different from controls at baseline. It therefore seems that the particularly vulnerable white matter tracts in AD show evidence of progression of pathology over a one year interval, even in established disease. Investigation of the pattern of change in DTI metrics at multiple different stages during the course of AD will be an important direction for future research. Another area will be the investigation into the involvement of other white matter tracts, such as the uncinate and superior longitudinal fasciculus. The patients in this study were all below the age of 72, representing a relatively young AD cohort. This reflects the referral pattern to the Cognitive Disorders Clinic from which they were recruited; as a tertiary centre run by neurologists, a high proportion of the patients referred to the clinic have early onset dementia. The benefit of studying a relatively young cohort is that they have fewer co-morbidities and it is therefore more likely that the imaging changes observed are secondary to AD rather than other or mixed pathologies such as vascular disease. However, it will be important for future studies to address whether our findings are generalisable to more elderly cohorts of AD patients. Although our linear regression models accounted for age and gender, the gender imbalance between the groups in the specificity and sensitivity experiments should be considered a limitation of the study.

Although we used WM tissue segmentation to measure the DTI parameters, there is still the risk of partial volume effects and CSF contamination in thin structures like the fornix. Future work should include strategies to correct for CSF-contamination, for example correcting on a voxel-wise basis using the Free Water Elimination (FWE) approach (Metzler-Baddeley et al., 2012; Pasternak et al., 2009).

There is an increasing need to develop biomarkers that reflect neural changes at the earliest stages of the disease in order to select appropriate individuals for trials of disease modifying therapies and, potentially, to look for therapeutic effects. With the design of a number of pre-symptomatic prevention trials for AD now underway (Bateman et al., 2011; Reiman et al., 2010), this issue is particularly timely. Whilst most studies in neurodegenerative disorders have historically focussed on grey matter, it is becoming clearer that white matter involvement occurs early on in the disease process, and DTI provides an opportunity to measure these changes. Measure of within-subject longitudinal change may be more sensitive biomarkers of neurodegeneration compared to

cross-sectional measures of a population. Thus, we have developed a method for the longitudinal study of DTI data in order to determine which white matter tracts become most affected by AD pathology over time with greater confidence.

Acknowledgments

This work was undertaken at UCLH/UCL who received a proportion of funding from the Department of Health's NIHR Biomedical Research Centres funding scheme. The Dementia Research Centre is an Alzheimer's Research UK Co-ordinating Centre and has also received equipment funding from Alzheimer's Research UK. NSR is supported by an MRC Clinical Research Training Fellowship (G0900421), NCF holds an MRC Senior Clinical Fellowship (G116/143) and is an NIHR senior investigator. MJC, MM and SO received funding from the EPSRC Programme Grant (EP/H046410/1) and the Computational Biology Research Centre (CBRC) Strategic Investment Award (Ref. 168). We are grateful to all of the study participants.

References

Agosta, F., Pievani, M., Sala, S., Geroldi, C., Galluzzi, S., Frisoni, G.B., Filippi, M., 2011. White matter damage in Alzheimer disease and its relationship to gray matter atrophy. Radiology 258, 853–863.

Andersson, J.L.R., Jenkinson, M., Smith, S., 2007. Non-linear registration aka spatial normalisation. Technical Report. FMRIB Centre, Oxford, United Kingdom (www.fmrib.ox.ac.uk/analysis/techrep).

Ardekani, S., Kumar, A., Bartzokis, G., Sinha, U., 2007. Exploratory voxel-based analysis of diffusion indices and hemispheric asymmetry in normal aging. Magn. Reson. Imaging 25, 154–167.

Arsigny, V., Fillard, P., Pennec, X., Ayache, N., 2006. Log-Euclidean metrics for fast and simple calculus on diffusion tensors. Magn. Reson. Med. 56, 411–421.

Bartlett, J.W., Frost, C., 2008. Reliability, repeatability and reproducibility: analysis of measurement errors in continuous variables. Ultrasound Obstet. Gynecol. 31, 466–475.

Basser, P.J., Pierpaoli, C., 1996. Microstructural and physiological features of tissues elucidated by quantitative-diffusion-tensor MRI. J. Magn. Reson. B 111, 209–219.

Bateman, R.J., Aisen, P.S., De Strooper, B., Fox, N.C., Lemere, C.A., Ringman, J.M., Salloway, S., Sperling, R.A., Windisch, M., Xiong, C., 2011. Autosomal-dominant Alzheimer's disease: a review and proposal for the prevention of Alzheimer's disease. Alzheimers Res. Ther. 3, 1.

Borroni, B., Brambati, S.M., Agosti, C., Gipponi, S., Bellelli, G., Gasparotti, R., Garibotto, V., Di Luca, M., Scifo, P., Perani, D., Padovani, A., 2007. Evidence of white matter changes on diffusion tensor imaging in frontotemporal dementia. Arch. Neurol. 64, 246–251.

Bozzali, M., Falini, A., Franceschi, M., Cercignani, M., Zuffi, M., Scotti, G., Comi, G., Filippi, M., 2002. White matter damage in Alzheimer's disease assessed in vivo using diffusion tensor magnetic resonance imaging. J. Neurol. Neurosurg. Psychiatry 72, 742–746.

Cardoso, M.J., Clarkson, M.J., Ridgway, G.R., Modat, M., Fox, N.C., Ourselin, S., Alzheimer's Disease Neuroimaging Initiative, 2011. LoAd: a locally adaptive cortical segmentation algorithm. NeuroImage 56, 1386–1397.

Catheline, G., Periot, O., Amirault, M., Braun, M., Dartigues, J.F., Auriacombe, S., Allard, M., 2010. Distinctive alterations of the cingulum bundle during aging and Alzheimer's disease. Neurobiol. Aging 31, 1582–1592.

Choo, I.H., Lee, D.Y., Oh, J.S., Lee, J.S., Lee, D.S., Song, I.C., Youn, J.C., Kim, S.G., Kim, K.W., Jhoo, J.H., Woo, J.I., 2010. Posterior cingulate cortex atrophy and regional cingulum disruption in mild cognitive impairment and Alzheimer's disease. Neurobiol. Aging 31, 772–779.

Cook, P.A., Bai, Y., Nedjati-Gilani, S., Seunarine, K.K., Hall, M.G., Parker, G.J., Alexander, D.C., 2006. Camino: open-source diffusion-MRI reconstruction and processing. 14th Scientific Meeting of the International Society for Magnetic Resonance in Medicine. Seattle, WA, USA, p. 2759.

Ding, B., Chen, K.M., Ling, H.W., Zhang, H., Chai, W.M., Li, X., Wang, T., 2008. Diffusion tensor imaging correlates with proton magnetic resonance spectroscopy in posterior cingulate region of patients with Alzheimer's disease. Dement. Geriatr. Cogn. Disord. 25, 218–225.

Douaud, G., Jbabdi, S., Behrens, T.E.J., Menke, R.A., Gass, A., Monsch, A.U., Rao, A., Whitcher, B., Kindlmann, G., Matthews, P.M., Smith, S., 2011. DTI measures in crossing-fibre areas: increased diffusion anisotropy reveals early white matter alteration in MCI and mild Alzheimer's disease. NeuroImage 55, 880–890.

Duan, J.H., Wang, H.Q., Xu, J., Lin, X., Chen, S.Q., Kang, Z., Yao, Z.B., 2006. White matter damage of patients with Alzheimer's disease correlated with the decreased cognitive function. Surg. Radiol. Anat. 28, 150–156.

Fellgiebel, A., Schermuly, I., Gerhard, A., Keller, I., Albrecht, J., Weibrich, C., Müller, M.J., Stoeter, P., 2008. Functional relevant loss of long association fibre tracts integrity in early Alzheimer's disease. Neuropsychologia 46, 1698–1706.

Hanyu, H., Imon, Y., Sakurai, H., Iwamoto, T., Takasaki, M., Shindo, H., Kakizaki, D., Abe, K., 1999. Regional differences in diffusion abnormality in cerebral white matter lesions in patients with vascular dementia of the Binswanger type and Alzheimer's disease. Eur. J. Neurol. 6, 195–203.

Head, D., Buckner, R.L., Shimony, J.S., Williams, L.E., Akbudak, E., Conturo, T.E., McAvoy, M., Morris, J.C., Snyder, A.Z., 2004. Differential vulnerability of anterior white matter in nondemented aging with minimal acceleration in dementia of the Alzheimer type: evidence from diffusion tensor imaging. Cereb. Cortex 14, 410–423.

Jenkinson, M., Smith, S., 2001. A global optimisation method for robust affine registration of brain images. Med. Image Anal. 5, 143–156.

Jones, D.K., Griffin, L.D., Alexander, D.C., Catani, M., Horsfield, M.A., Howard, R., Williams, S.C.R., 2002. Spatial normalization and averaging of diffusion tensor MRI data sets. NeuroImage 17, 592–617.

Keihaninejad, S., Ryan, N., Malone, I.B., Modat, M., Cash, D., Ridgway, G., Zhang, H., Fox, N.C., Ourselin, S., 2012. The importance of group-wise registration in Tract Based Spatial Statistics study of neurodegeneration: a simulation study in Alzheimer's disease. PLoS One 7, e45996.

Kiuchi, K., Morikawa, M., Taoka, T., Nagashima, T., Yamauchi, T., Makinodan, M., Norimoto, K., Hashimoto, K., Kosaka, J., Inoue, Y., Inoue, M., Kichikawa, K., Kishimoto, T., 2009. Abnormalities of the uncinate fasciculus and posterior cingulate fasciculus in mild cognitive impairment and early Alzheimer's disease: a diffusion tensor tractography study. Brain Res. 1287, 184–191.

Liu, Y., Spulber, G., Lehtimäki, K.K., Könönen, M., Hallikainen, I., Gröhn, H., Kivipelto, M., Hallikainen, M., Vanninen, R., Soininen, H., 2011. Diffusion tensor imaging and tract-based spatial statistics in Alzheimer's disease and mild cognitive impairment. Neurobiol. Aging 32, 1558–1571.

Matsuo, K., Mizuno, T., Yamada, K., Akazawa, K., Kasai, T., Kondo, M., Mori, S., Nishimura, T., Nakagawa, M., 2008. Cerebral white matter damage in frontotemporal dementia assessed by diffusion tensor tractography. Neuroradiology 50, 605–611.

Metzler-Baddeley, C., O'Sullivan, M.J., Bells, S., Pasternak, O., Jones, D.K., 2012. How and how not to correct for CSF-contamination in diffusion MRI. NeuroImage 59, 1394–1403.

Mielke, M.M., Kozauer, N.A., Chan, K.C.G., George, M., Toroney, J., Zerrate, M., Bandeen-Roche, K., Wang, M.C., Vanzijl, P., Pekar, J.J., Mori, S., Lyketsos, C.G., Albert, M., 2009. Regionally-specific diffusion tensor imaging in mild cognitive impairment and Alzheimer's disease. NeuroImage 46, 47–55.

Mielke, M.M., Okonkwo, O.C., Oishi, K., Mori, S., Tighe, S., Miller, M.I., Ceritoglu, C., Brown, T., Albert, M., Lyketsos, C.G., 2012. Fornix integrity and hippocampal volume predict memory decline and progression to Alzheimer's disease. Alzheimers Dement. 8, 105–113.

Modat, M., Ridgway, G.R., Taylor, Z.A., Lehmann, M., Barnes, J., Hawkes, D.J., Fox, N.C., Ourselin, S., 2010. Fast free-form deformation using graphics processing units. Comput. Methods Programs Biomed. 98, 278–284.

Mori, S., Wakana, S., Nagae-Poetscher, L., van Zijl, P., 2005. MRI atlas of Human White Matter. Elsevier B. V.

Nakata, Y., Sato, N., Abe, O., Shikakura, S., Arima, K., Furuta, N., Uno, M., Hirai, S., Masutani, Y., Ohtomo, K., Aoki, S., 2008. Diffusion abnormality in posterior cingulate fiber tracts in Alzheimer's disease: tract-specific analysis. Radiat. Med. 26, 466–473.

Oishi, K., Mielke, M.M., Albert, M., Lyketsos, C.G., Mori, S., 2011. The fornix sign: a potential sign for Alzheimer's disease based on diffusion tensor imaging. J. Neuroimaging 22 (4), 365–374.

Park, H.J., Kubicki, M., Shenton, M.E., Guimond, A., McCarley, R.W., Maier, S.E., Kikinis, R., Jolesz, F.A., Westin, C.F., 2003. Spatial normalization of diffusion tensor MRI using multiple channels. NeuroImage 20, 1995–2009.

Pasternak, O., Sochen, N., Gur, Y., Intrator, N., Assaf, Y., 2009. Free water elimination and mapping from diffusion MRI. Magn. Reson. Med. 62, 717–730.

Pfefferbaum, A., Adalsteinsson, E., Sullivan, E.V., 2003. Replicability of diffusion tensor imaging measurements of fractional anisotropy and trace in brain. J. Magn. Reson. Imaging 18, 427–433.

Pierpaoli, C., Jezzard, P., Basser, P.J., Barnett, A., Di Chiro, G., 1996. Diffusion tensor MR imaging of the human brain. Radiology 201, 637–648.

Reiman, E.M., Langbaum, J.B.S., Tariot, P.N., 2010. Alzheimer's prevention initiative: a proposal to evaluate presymptomatic treatments as quickly as possible. Biomark. Med. 4, 3–14.

Reuter, M., Schmansky, N.J., Rosas, H.D., Fischl, B., 2012. Within-subject template estimation for unbiased longitudinal image analysis. NeuroImage 61, 1402–1418.

Rose, S.E., Chen, F., Chalk, J.B., Zelaya, F.O., Strugnell, W.E., Benson, M., Semple, J., Doddrell, D.M., 2000. Loss of connectivity in Alzheimer's disease: an evaluation of white matter tract integrity with colour coded MR diffusion tensor imaging. J. Neurol. Neurosurg. Psychiatry 69, 528–530.

Scahill, R.I., Schott, J.M., Stevens, J.M., Rossor, M.N., Fox, N.C., 2002. Mapping the evolution of regional atrophy in Alzheimer's disease: unbiased analysis of fluid-registered serial MRI. Proc. Natl. Acad. Sci. U. S. A. 99, 4703–4707.

Sexton, C.E., Mackay, C.E., Lonie, J.A., Bastin, M.E., Terrière, E., O'Carroll, R.E., Ebmeier, K.P., 2010. MRI correlates of episodic memory in Alzheimer's disease, mild cognitive impairment, and healthy aging. Psychiatry Res. 184, 57–62.

Smith, S.M., Jenkinson, M., Woolrich, M.W., Beckmann, C.F., Behrens, T.E.J., Johansen-Berg, H., Bannister, P.R., De Luca, M., Drobnjak, I., Flitney, D.E., Niazy, R.K., Saunders, J., Vickers, J., Zhang, Y., De Stefano, N., Brady, J.M., Matthews, P.M., 2004. Advances in functional and structural MR image analysis and implementation as FSL. NeuroImage 23 (Suppl. 1), S208–S219.

Smith, S.M., Jenkinson, M., Johansen-Berg, H., Rueckert, D., Nichols, T.E., Mackay, C.E., Watkins, K.E., Ciccarelli, O., Cader, M.Z., Matthews, P.M., Behrens, T.E.J., 2006. Tract-based spatial statistics: voxelwise analysis of multi-subject diffusion data. NeuroImage 31, 1487–1505.

Sugihara, S., Kinoshita, T., Matsusue, E., Fujii, S., Ogawa, T., 2004. Usefulness of diffusion tensor imaging of white matter in Alzheimer disease and vascular dementia. Acta Radiol. 45, 658–663.

Takahashi, S., Yonezawa, H., Takahashi, J., Kudo, M., Inoue, T., Tohgi, H., 2002. Selective reduction of diffusion anisotropy in white matter of Alzheimer disease brains measured by 3.0 Tesla magnetic resonance imaging. Neurosci. Lett. 332, 45–48.

Teipel, S.J., Meindl, T., Wagner, M., Stieltjes, B., Reuter, S., Hauenstein, K.H., Filippi, M., Ernemann, U., Reiser, M.F., Hampel, H., 2010. Longitudinal changes in fiber tract integrity in healthy aging and mild cognitive impairment: a DTI follow-up study. J. Alzheimers Dis. 22, 507–522.

Wang, Y., Gupta, A., Liu, Z., Zhang, H., Escolar, M.L., Gilmore, J.H., Gouttard, S., Fillard, P., Maltbie, E., Gerig, G., Styner, M., 2011. DTI registration in atlas based fiber analysis of infantile Krabbe disease. NeuroImage 55, 1577–1586.

Xie, S., Xiao, J.X., Gong, G.L., Zang, Y.F., Wang, Y.H., Wu, H.K., Jiang, X.X., 2006. Voxel-based detection of white matter abnormalities in mild Alzheimer disease. Neurology 66, 1845–1849.

Yushkevich, P.A., Avants, B.B., Das, S.R., Pluta, J., Altinay, M., Craige, C., Alzheimer's Disease Neuroimaging Initiative, 2010. Bias in estimation of hippocampal atrophy using deformation-based morphometry arises from asymmetric global normalization: an illustration in ADNI 3 T MRI data. NeuroImage 50, 434–445.

Zatorre, R.J., Fields, R.D., Johansen-Berg, H., 2012. Plasticity in gray and white: neuroimaging changes in brain structure during learning. Nat. Neurosci. 15, 528–536.

Zhang, H., Yushkevich, P.A., Alexander, D.C., Gee, J.C., 2006. Deformable registration of diffusion tensor MR images with explicit orientation optimization. Med. Image Anal. 10, 764–785.

Zhang, H., Avants, B.B., Yushkevich, P.A., Woo, J.H., Wang, S., McCluskey, L.F., Elman, L.B., Melhem, E.R., Gee, J.C., 2007a. High-dimensional spatial normalization of diffusion tensor images improves the detection of white matter differences: an example study using amyotrophic lateral sclerosis. IEEE Trans. Med. Imaging 26, 1585–1597.

Zhang, Y., Schuff, N., Jahng, G.H., Bayne, W., Mori, S., Schad, L., Mueller, S., Du, A.T., Kramer, J.H., Yaffe, K., Chui, H., Jagust, W.J., Miller, B.L., Weiner, M.W., 2007b. Diffusion tensor imaging of cingulum fibers in mild cognitive impairment and Alzheimer disease. Neurology 68, 13–19.

Zhang, H., Yushkevich, P.A., Rueckert, D., Gee, J.C., 2007c. Unbiased white matter atlas construction using diffusion tensor images. Med Image Comput Comput Assist Interv (MICCAI), pp. 211–218.